

Study of double parton interactions in diphoton + dijet events in $p\bar{p}$ collisions at $\sqrt{s} = 1.96$ TeV

V.M. Abazov,³¹ B. Abbott,⁶⁷ B.S. Acharya,²⁵ M. Adams,⁴⁶ T. Adams,⁴⁴ J.P. Agnew,⁴¹ G.D. Alexeev,³¹ G. Alkhazov,³⁵ A. Alton^a,⁵⁶ A. Askew,⁴⁴ S. Atkins,⁵⁴ K. Augsten,⁷ V. Aushev,³⁸ Y. Aushev,³⁸ C. Avila,⁵ F. Badaud,¹⁰ L. Bagby,⁴⁵ B. Baldin,⁴⁵ D.V. Bandurin,⁷⁴ S. Banerjee,²⁵ E. Barberis,⁵⁵ P. Baringer,⁵³ J.F. Bartlett,⁴⁵ U. Bassler,¹⁵ V. Bazterra,⁴⁶ A. Bean,⁵³ M. Begalli,² L. Bellantoni,⁴⁵ S.B. Beri,²³ G. Bernardi,¹⁴ R. Bernhard,¹⁹ I. Bertram,³⁹ M. Besançon,¹⁵ R. Beuselinck,⁴⁰ P.C. Bhat,⁴⁵ S. Bhatia,⁵⁸ V. Bhatnagar,²³ G. Blazey,⁴⁷ S. Blessing,⁴⁴ K. Bloom,⁵⁹ A. Boehnlein,⁴⁵ D. Boline,⁶⁴ E.E. Boos,³³ G. Borissov,³⁹ M. Borysova^l,³⁸ A. Brandt,⁷¹ O. Brandt,²⁰ R. Brock,⁵⁷ A. Bross,⁴⁵ D. Brown,¹⁴ X.B. Bu,⁴⁵ M. Buehler,⁴⁵ V. Buescher,²¹ V. Bunichev,³³ S. Burdin^b,³⁹ C.P. Buszello,³⁷ E. Camacho-Pérez,²⁸ B.C.K. Casey,⁴⁵ H. Castilla-Valdez,²⁸ S. Caughron,⁵⁷ S. Chakrabarti,⁶⁴ K.M. Chan,⁵¹ A. Chandra,⁷³ E. Chapon,¹⁵ G. Chen,⁵³ S.W. Cho,²⁷ S. Choi,²⁷ B. Choudhary,²⁴ S. Cihangir,⁴⁵ D. Claes,⁵⁹ J. Clutter,⁵³ M. Cooke^k,⁴⁵ W.E. Cooper,⁴⁵ M. Corcoran,⁷³ F. Couderc,¹⁵ M.-C. Cousinou,¹² J. Cuth,²¹ D. Cutts,⁷⁰ A. Das,⁷² G. Davies,⁴⁰ S.J. de Jong,^{29,30} E. De La Cruz-Burelo,²⁸ F. Déliot,¹⁵ R. Demina,⁶³ D. Denisov,⁴⁵ S.P. Denisov,³⁴ S. Desai,⁴⁵ C. Deterre^c,⁴¹ K. DeVaughan,⁵⁹ H.T. Diehl,⁴⁵ M. Diesburg,⁴⁵ P.F. Ding,⁴¹ A. Dominguez,⁵⁹ A. Dubey,²⁴ L.V. Dudko,³³ A. Duperrin,¹² S. Dutt,²³ M. Eads,⁴⁷ D. Edmunds,⁵⁷ J. Ellison,⁴³ V.D. Elvira,⁴⁵ Y. Enari,¹⁴ H. Evans,⁴⁹ A. Evdokimov,⁴⁶ V.N. Evdokimov,³⁴ A. Fauré,¹⁵ L. Feng,⁴⁷ T. Ferbel,⁶³ F. Fiedler,²¹ F. Filthaut,^{29,30} W. Fisher,⁵⁷ H.E. Fisk,⁴⁵ M. Fortner,⁴⁷ H. Fox,³⁹ J. Franc,⁷ S. Fuess,⁴⁵ P.H. Garbincius,⁴⁵ A. Garcia-Bellido,⁶³ J.A. García-González,²⁸ P. Gaspar,² V. Gavrilov,³² W. Geng,^{12,57} C.E. Gerber,⁴⁶ Y. Gershtein,⁶⁰ G. Ginther,⁴⁵ O. Gogota,³⁸ G. Golovanov,³¹ P.D. Grannis,⁶⁴ S. Greder,¹⁶ H. Greenlee,⁴⁵ G. Grenier,¹⁷ Ph. Gris,¹⁰ J.-F. Grivaz,¹³ A. Grohsjean^c,¹⁵ S. Grünendahl,⁴⁵ M.W. Grünewald,²⁶ T. Guillemain,¹³ G. Gutierrez,⁴⁵ P. Gutierrez,⁶⁷ J. Haley,⁶⁸ L. Han,⁴ K. Harder,⁴¹ A. Harel,⁶³ J.M. Hauptman,⁵² J. Hays,⁴⁰ T. Head,⁴¹ T. Hebbeker,¹⁸ D. Hedin,⁴⁷ H. Hegab,⁶⁸ A.P. Heinson,⁴³ U. Heintz,⁷⁰ C. Hensel,¹ I. Heredia-De La Cruz^d,²⁸ K. Herner,⁴⁵ G. Hesketh^f,⁴¹ M.D. Hildreth,⁵¹ R. Hirosky,⁷⁴ T. Hoang,⁴⁴ J.D. Hobbs,⁶⁴ B. Hoeneisen,⁹ J. Hogan,⁷³ M. Hohlfeld,²¹ J.L. Holzbauer,⁵⁸ I. Howley,⁷¹ Z. Hubacek,^{7,15} V. Hynek,⁷ I. Iashvili,⁶² Y. Ilchenko,⁷² R. Illingworth,⁴⁵ A.S. Ito,⁴⁵ S. Jabeen^m,⁴⁵ M. Jaffré,¹³ A. Jayasinghe,⁶⁷ M.S. Jeong,²⁷ R. Jesik,⁴⁰ P. Jiang[†],⁴ K. Johns,⁴² E. Johnson,⁵⁷ M. Johnson,⁴⁵ A. Jonckheere,⁴⁵ P. Jonsson,⁴⁰ J. Joshi,⁴³ A.W. Jung^o,⁴⁵ A. Juste,³⁶ E. Kajfasz,¹² D. Karmanov,³³ I. Katsanos,⁵⁹ M. Kaur,²³ R. Kehoe,⁷² S. Kermiche,¹² N. Khalatyan,⁴⁵ A. Khanov,⁶⁸ A. Kharchilava,⁶² Y.N. Kharzheev,³¹ I. Kiselevich,³² J.M. Kohli,²³ A.V. Kozelov,³⁴ J. Kraus,⁵⁸ A. Kumar,⁶² A. Kupco,⁸ T. Kurča,¹⁷ V.A. Kuzmin,³³ S. Lammers,⁴⁹ P. Lebrun,¹⁷ H.S. Lee,²⁷ S.W. Lee,⁵² W.M. Lee,⁴⁵ X. Lei,⁴² J. Lellouch,¹⁴ D. Li,¹⁴ H. Li,⁷⁴ L. Li,⁴³ Q.Z. Li,⁴⁵ J.K. Lim,²⁷ D. Lincoln,⁴⁵ J. Linnemann,⁵⁷ V.V. Lipaev,³⁴ R. Lipton,⁴⁵ H. Liu,⁷² Y. Liu,⁴ A. Lobodenko,³⁵ M. Lokajicek,⁸ R. Lopes de Sa,⁴⁵ R. Luna-Garcia^g,²⁸ A.L. Lyon,⁴⁵ A.K.A. Maciel,¹ R. Madar,¹⁹ R. Magaña-Villalba,²⁸ S. Malik,⁵⁹ V.L. Malyshev,³¹ J. Mansour,²⁰ J. Martínez-Ortega,²⁸ R. McCarthy,⁶⁴ C.L. McGivern,⁴¹ M.M. Meijer,^{29,30} A. Melnitchouk,⁴⁵ D. Menezes,⁴⁷ P.G. Mercadante,³ M. Merkin,³³ A. Meyer,¹⁸ J. Meyerⁱ,²⁰ F. Miconi,¹⁶ N.K. Mondal,²⁵ M. Mulhearn,⁷⁴ E. Nagy,¹² M. Narain,⁷⁰ R. Nayyar,⁴² H.A. Neal,⁵⁶ J.P. Negret,⁵ P. Neustroev,³⁵ H.T. Nguyen,⁷⁴ T. Nunnemann,²² J. Orduna,⁷³ N. Osman,¹² J. Osta,⁵¹ A. Pal,⁷¹ N. Parashar,⁵⁰ V. Parihar,⁷⁰ S.K. Park,²⁷ R. Partridge^e,⁷⁰ N. Parua,⁴⁹ A. Patwa^j,⁶⁵ B. Penning,⁴⁰ M. Perfilov,³³ Y. Peters,⁴¹ K. Petridis,⁴¹ G. Petrillo,⁶³ P. Pétroff,¹³ M.-A. Pleier,⁶⁵ V.M. Podstavkov,⁴⁵ A.V. Popov,³⁴ M. Prewitt,⁷³ D. Price,⁴¹ N. Prokopenko,³⁴ J. Qian,⁵⁶ A. Quadt,²⁰ B. Quinn,⁵⁸ P.N. Ratoff,³⁹ I. Razumov,³⁴ I. Ripp-Baudot,¹⁶ F. Rizatdinova,⁶⁸ M. Rominsky,⁴⁵ A. Ross,³⁹ C. Royon,⁸ P. Rubinov,⁴⁵ R. Ruchti,⁵¹ G. Sajot,¹¹ A. Sánchez-Hernández,²⁸ M.P. Sanders,²² A.S. Santos^h,¹ G. Savage,⁴⁵ M. Savitskyi,³⁸ L. Sawyer,⁵⁴ T. Scanlon,⁴⁰ R.D. Schamberger,⁶⁴ Y. Scheglov,³⁵ H. Schellman,^{69,48} M. Schott,²¹ C. Schwanenberger,⁴¹ R. Schwienhorst,⁵⁷ J. Sekaric,⁵³ H. Severini,⁶⁷ E. Shabalina,²⁰ V. Shary,¹⁵ S. Shaw,⁴¹ A.A. Shchukin,³⁴ V. Simak,⁷ P. Skubic,⁶⁷ P. Slattery,⁶³ D. Smirnov,⁵¹ G.R. Snow,⁵⁹ J. Snow,⁶⁶ S. Snyder,⁶⁵ S. Söldner-Rembold,⁴¹ L. Sonnenschein,¹⁸ K. Soustruznik,⁶ J. Stark,¹¹ N. Stefaniuk,³⁸ D.A. Stoyanova,³⁴ M. Strauss,⁶⁷ L. Suter,⁴¹ P. Svoisky,⁷⁴ M. Titov,¹⁵ V.V. Tokmenin,³¹ Y.-T. Tsai,⁶³ D. Tsybychev,⁶⁴ B. Tuchming,¹⁵ C. Tully,⁶¹ L. Uvarov,³⁵ S. Uvarov,³⁵ S. Uzunyan,⁴⁷ R. Van Kooten,⁴⁹ W.M. van Leeuwen,²⁹ N. Varelas,⁴⁶ E.W. Varnes,⁴² I.A. Vasilyev,³⁴ A.Y. Verkheev,³¹ L.S. Vertogradov,³¹ M. Verzocchi,⁴⁵ M. Vesterinen,⁴¹ D. Vilanova,¹⁵ P. Vokac,⁷ H.D. Wahl,⁴⁴ M.H.L.S. Wang,⁴⁵ J. Warchol,⁵¹ G. Watts,⁷⁵ M. Wayne,⁵¹ J. Weichert,²¹ L. Welty-Rieger,⁴⁸ M.R.J. Williamsⁿ,⁴⁹ G.W. Wilson,⁵³ M. Wobisch,⁵⁴ D.R. Wood,⁵⁵ T.R. Wyatt,⁴¹ Y. Xie,⁴⁵ R. Yamada,⁴⁵ S. Yang,⁴ T. Yasuda,⁴⁵ Y.A. Yatsunenko,³¹ W. Ye,⁶⁴ Z. Ye,⁴⁵ H. Yin,⁴⁵ K. Yip,⁶⁵ S.W. Youn,⁴⁵

J.M. Yu,⁵⁶ J. Zennaro,⁶² T.G. Zhao,⁴¹ B. Zhou,⁵⁶ J. Zhu,⁵⁶ M. Zielinski,⁶³ D. Zieminska,⁴⁹ and L. Zivkovic¹⁴

(The D0 Collaboration*)

¹LAFEX, Centro Brasileiro de Pesquisas Físicas, Rio de Janeiro, Brazil

²Universidade do Estado do Rio de Janeiro, Rio de Janeiro, Brazil

³Universidade Federal do ABC, Santo André, Brazil

⁴University of Science and Technology of China, Hefei, People's Republic of China

⁵Universidad de los Andes, Bogotá, Colombia

⁶Charles University, Faculty of Mathematics and Physics,
Center for Particle Physics, Prague, Czech Republic

⁷Czech Technical University in Prague, Prague, Czech Republic

⁸Institute of Physics, Academy of Sciences of the Czech Republic, Prague, Czech Republic

⁹Universidad San Francisco de Quito, Quito, Ecuador

¹⁰LPC, Université Blaise Pascal, CNRS/IN2P3, Clermont, France

¹¹LPSC, Université Joseph Fourier Grenoble 1, CNRS/IN2P3,

Institut National Polytechnique de Grenoble, Grenoble, France

¹²CPPM, Aix-Marseille Université, CNRS/IN2P3, Marseille, France

¹³LAL, Univ. Paris-Sud, CNRS/IN2P3, Université Paris-Saclay, Orsay, France

¹⁴LPNHE, Universités Paris VI and VII, CNRS/IN2P3, Paris, France

¹⁵CEA, Irfu, SPP, Saclay, France

¹⁶IPHC, Université de Strasbourg, CNRS/IN2P3, Strasbourg, France

¹⁷IPNL, Université Lyon 1, CNRS/IN2P3, Villeurbanne, France and Université de Lyon, Lyon, France

¹⁸III. Physikalisches Institut A, RWTH Aachen University, Aachen, Germany

¹⁹Physikalisches Institut, Universität Freiburg, Freiburg, Germany

²⁰II. Physikalisches Institut, Georg-August-Universität Göttingen, Göttingen, Germany

²¹Institut für Physik, Universität Mainz, Mainz, Germany

²²Ludwig-Maximilians-Universität München, München, Germany

²³Panjab University, Chandigarh, India

²⁴Delhi University, Delhi, India

²⁵Tata Institute of Fundamental Research, Mumbai, India

²⁶University College Dublin, Dublin, Ireland

²⁷Korea Detector Laboratory, Korea University, Seoul, Korea

²⁸CINVESTAV, Mexico City, Mexico

²⁹Nikhef, Science Park, Amsterdam, the Netherlands

³⁰Radboud University Nijmegen, Nijmegen, the Netherlands

³¹Joint Institute for Nuclear Research, Dubna, Russia

³²Institute for Theoretical and Experimental Physics, Moscow, Russia

³³Moscow State University, Moscow, Russia

³⁴Institute for High Energy Physics, Protvino, Russia

³⁵Petersburg Nuclear Physics Institute, St. Petersburg, Russia

³⁶Institució Catalana de Recerca i Estudis Avançats (ICREA) and Institut de Física d'Altes Energies (IFAE), Barcelona, Spain

³⁷Uppsala University, Uppsala, Sweden

³⁸Taras Shevchenko National University of Kyiv, Kiev, Ukraine

³⁹Lancaster University, Lancaster LA1 4YB, United Kingdom

⁴⁰Imperial College London, London SW7 2AZ, United Kingdom

⁴¹The University of Manchester, Manchester M13 9PL, United Kingdom

⁴²University of Arizona, Tucson, Arizona 85721, USA

⁴³University of California Riverside, Riverside, California 92521, USA

⁴⁴Florida State University, Tallahassee, Florida 32306, USA

⁴⁵Fermi National Accelerator Laboratory, Batavia, Illinois 60510, USA

⁴⁶University of Illinois at Chicago, Chicago, Illinois 60607, USA

⁴⁷Northern Illinois University, DeKalb, Illinois 60115, USA

⁴⁸Northwestern University, Evanston, Illinois 60208, USA

⁴⁹Indiana University, Bloomington, Indiana 47405, USA

⁵⁰Purdue University Calumet, Hammond, Indiana 46323, USA

⁵¹University of Notre Dame, Notre Dame, Indiana 46556, USA

⁵²Iowa State University, Ames, Iowa 50011, USA

⁵³University of Kansas, Lawrence, Kansas 66045, USA

⁵⁴Louisiana Tech University, Ruston, Louisiana 71272, USA

⁵⁵Northeastern University, Boston, Massachusetts 02115, USA

⁵⁶University of Michigan, Ann Arbor, Michigan 48109, USA

⁵⁷Michigan State University, East Lansing, Michigan 48824, USA

⁵⁸University of Mississippi, University, Mississippi 38677, USA

⁵⁹University of Nebraska, Lincoln, Nebraska 68588, USA

- ⁶⁰*Rutgers University, Piscataway, New Jersey 08855, USA*
⁶¹*Princeton University, Princeton, New Jersey 08544, USA*
⁶²*State University of New York, Buffalo, New York 14260, USA*
⁶³*University of Rochester, Rochester, New York 14627, USA*
⁶⁴*State University of New York, Stony Brook, New York 11794, USA*
⁶⁵*Brookhaven National Laboratory, Upton, New York 11973, USA*
⁶⁶*Langston University, Langston, Oklahoma 73050, USA*
⁶⁷*University of Oklahoma, Norman, Oklahoma 73019, USA*
⁶⁸*Oklahoma State University, Stillwater, Oklahoma 74078, USA*
⁶⁹*Oregon State University, Corvallis, Oregon 97331, USA*
⁷⁰*Brown University, Providence, Rhode Island 02912, USA*
⁷¹*University of Texas, Arlington, Texas 76019, USA*
⁷²*Southern Methodist University, Dallas, Texas 75275, USA*
⁷³*Rice University, Houston, Texas 77005, USA*
⁷⁴*University of Virginia, Charlottesville, Virginia 22904, USA*
⁷⁵*University of Washington, Seattle, Washington 98195, USA*
(Dated: March 17, 2016)

We use a sample of diphoton + dijet events to measure the effective cross section of double parton interactions, which characterizes the area containing the interacting partons in proton-antiproton collisions, and find it to be $\sigma_{\text{eff}} = 19.3 \pm 1.4(\text{stat}) \pm 7.8(\text{syst})$ mb. The sample was collected by the D0 detector at the Fermilab Tevatron collider in $p\bar{p}$ collisions at $\sqrt{s} = 1.96$ TeV and corresponds to an integrated luminosity of 8.7 fb^{-1} .

PACS numbers: 14.20.Dh, 13.85.Qk, 12.38.Qk

I. INTRODUCTION

Many features of high energy inelastic hadron collisions are directly dependent on the parton structure of hadrons, which is not yet completely understood either at the theoretical or experimental levels. Studies of this structure generally rely on a theoretical model of inelastic scattering of high energy nucleons, where a single parton (quark or gluon from one nucleon or a lepton in Deep Inelastic Scattering (DIS) experiments) interacts with a single parton from another nucleon. In this approach, the other “spectator” partons which do not take part in a hard $2 \rightarrow 2$ parton collision are included in the so-called “underlying event.”

Information regarding the abundance of simultaneous double parton (DP) interactions comprising two separate hard parton scatterings within a single hadron-hadron collision [1–16] is a subject of great interest, because

the growing LHC luminosity provides an opportunity to search for signals from new physics for which the DP events constitute a significant background, especially in the multijet final state. For example, processes such as the associated production of the Higgs and W bosons, with the Higgs boson decaying into a pair of b quarks, have substantial DP backgrounds [17].

Several relevant measurements have been already performed using hadron collisions at $\sqrt{s} = 63$ GeV [18], $\sqrt{s} = 630$ GeV [19], $\sqrt{s} = 1.8$ TeV [20, 21], $\sqrt{s} = 1.96$ TeV [22–26], $\sqrt{s} = 7$ TeV [27–30], and $\sqrt{s} = 8$ TeV [27]. The first three measurements utilize a four jet final state, where the transverse momentum of the jets in each jet pair is balanced, resulting in the jets produced at almost opposite azimuthal angles. AFS [18] has found (for jet transverse energy $E_T^{\text{jet}} > 4$ GeV and pseudorapidity [31] $|\eta^{\text{jet}}| \leq 1$) the ratio of DP/2jet cross sections to be $6\% \pm 1.5\%(\text{stat}) \pm 2.2\%(\text{syst})$. UA2 [19] retained only jet clusters with transverse momentum $p_T^{\text{jet}} > 15$ GeV and $|\eta^{\text{jet}}| < 2$ and set a 95% C.L. limit on the value of the DP cross section, $\sigma_{\text{DP}} \leq 0.82$ nb. The CDF measurement of the DP fraction in four jet events [20] found a DP cross section of $\sigma_{\text{DP}} = 63_{-28}^{+32}$ nb for jets having $p_T^{\text{jet}} \geq 25$ GeV and $|\eta^{\text{jet}}| \leq 3.5$. Additional CDF and D0 measurements [21–24] are based on the DP process comprising two parton scatterings with one of them having a dijet final state and the other having a γ +jet or $\gamma + b(c)$ -jet final state. D0 and LHCb measurements [25–27, 30] probe the final states containing heavy quarkonia. In Refs. [26, 27], the production of the studied final states in DP scattering is predicted to dominate the production in a single parton (SP) scattering. In this paper, we report the first measurement of DP scattering in the diphoton-dijet ($\gamma\gamma + jj$) channel.

*with visitors from ^aAugustana College, Sioux Falls, SD, USA, ^bThe University of Liverpool, Liverpool, UK, ^cDESY, Hamburg, Germany, ^dCONACyT, Mexico City, Mexico, ^eSLAC, Menlo Park, CA, USA, ^fUniversity College London, London, UK, ^gCentro de Investigacion en Computacion - IPN, Mexico City, Mexico, ^hUniversidade Estadual Paulista, São Paulo, Brazil, ⁱKarlsruher Institut für Technologie (KIT) - Steinbuch Centre for Computing (SCC), D-76128 Karlsruhe, Germany, ^jOffice of Science, U.S. Department of Energy, Washington, D.C. 20585, USA, ^kAmerican Association for the Advancement of Science, Washington, D.C. 20005, USA, ^lKiev Institute for Nuclear Research, Kiev, Ukraine, ^mUniversity of Maryland, College Park, MD 20742, USA, ⁿEuropean Organization for Nuclear Research (CERN), Geneva, Switzerland and ^oPurdue University, West Lafayette, IN 47907, USA. [†]Deceased.

As shown experimentally in Refs. [20–22] and described in Ref. [32], the substitution of one of the two dijet parton processes by a photon jet or a diphoton process leads to about an order of magnitude increase in the ratio of the DP cross section to the cross section of the SP scattering for the production of the same final state. This improves the ability to characterize the DP contribution in the data. Additionally, a technique for extracting an important physical parameter, σ_{eff} , has been proposed in Ref. [21]. This method uses only quantities obtained from data analysis and minimizes theoretical assumptions that were used in the previous measurements.

The parameter, σ_{eff} , is related to the distance between partons in the nucleon [3–6, 8, 9, 18–21],

$$\sigma_{\text{eff}}^{-1} = \int d^2\beta [F(\beta)]^2 \quad (1)$$

with $F(\beta) = \int f(\mathbf{b})f(\mathbf{b} - \beta)d^2b$, where β is the vector impact parameter of the two colliding hadrons and $f(\mathbf{b})$ is a function describing the transverse spatial distribution of the partonic matter inside a hadron [8–10]. The $f(\mathbf{b})$ may depend on the parton flavor.

The cross section for double parton scattering, σ_{DP} , is related to σ_{eff} [19–21] for the 2- γ and 2-jet process as

$$\sigma_{\text{DP}} \equiv \frac{m}{2} \frac{\sigma^{\gamma\gamma} \sigma^{jj}}{\sigma_{\text{eff}}}. \quad (2)$$

The factor of 1/2 is due to the assumption that the probability of multiple parton interactions inside the proton follows a Poisson distribution [7]. For this analysis, the factor m is equal to 2 because the diphoton and double jet production processes are distinguishable (in the case of 4-jet production, i.e. two dijet processes, $m = 1$). Table I summarizes the available data on the measurements of σ_{eff} . The goal of this study is to obtain the DP rate and the effective cross section in the diphoton+dijet final state.

The main contributions to diphoton production at the Tevatron are from the $q\bar{q} \rightarrow \gamma\gamma$ and $gg \rightarrow \gamma\gamma$ via direct 2 \rightarrow 2 partonic processes, as well as from bremsstrahlung processes with single and double parton-to-photon fragmentations. Figure 1 shows representative Feynman diagrams for DP diphoton plus dijet production. For dijet scattering, the $gg \rightarrow gg$ process is shown, because it is dominant in the jet kinematic range studied in this analysis.

Figure 2 shows the relative fraction of the $gg \rightarrow \gamma\gamma$ contribution to the total diphoton cross section, which is a combination of $q\bar{q} \rightarrow \gamma\gamma$ and $gg \rightarrow \gamma\gamma$ processes. For this analysis, which restricts the transverse momenta of each of the two leading jets to the range of 15–40 GeV and the transverse momenta of each of the two leading photons to be above 15 GeV, the $q\bar{q}$ scattering significantly dominates the gg process, with $q\bar{q}$ fraction of about 70%–80%.

The outline of the paper is as follows. Section II briefly describes the method for extracting σ_{eff} proposed in

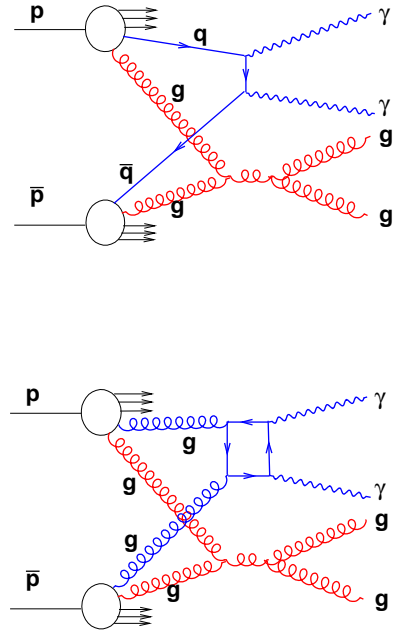


FIG. 1: Schematic view of DP scattering processes producing $\gamma\gamma$ +dijet final state. The $\gamma\gamma$ process is shown for the $q\bar{q}$ scattering (above, light, blue online) and box gg diagram (below, light, blue online). The additional dijet scattering is a darker diagram (red online).

Ref. [21]. Section III introduces the D0 detector and data samples. Section IV describes the signal and background models used in this measurement. Section V discusses the discriminating variable used to identify a data sample with an enhanced population of DP events. The procedure for finding the fraction of DP events is given in Sec. VIA. Section VIB contains a description of the analogous procedure used to measure the fraction of events with double $p\bar{p}$ interactions. A summary of the efficiencies required for the measurement is presented in Sec. VII. In Sec. VIII, we calculate the effective cross section, σ_{eff} , for the diphoton+dijet final state. The conclusions and outlook are presented in Sec. IX.

II. TECHNIQUE FOR EXTRACTING σ_{eff} FROM DATA

The technique for extracting σ_{eff} has been used in a number of earlier measurements [21, 22, 24]. To avoid using theoretical predictions for the SP diphoton and dijet cross sections, the technique is based on a comparison of the number of $\gamma\gamma$ +dijet events produced in DP interactions in single $p\bar{p}$ collisions to the number of $\gamma\gamma$ +dijet events produced in two separate $p\bar{p}$ collisions. In the lat-

TABLE I: Summary of the results, experimental parameters, and event selection criteria for the double parton analyses performed by the AFS, UA2, CDF, D0, ATLAS, CMS, and LHCb Collaborations (no uncertainties are available for the AFS result).

	\sqrt{s} (GeV)	Final state	p_T^{min} (GeV/c)	η range	Result
AFS, 1986 [18]	63	4 jets	$p_T^{\text{jet}} > 4$	$ \eta^{\text{jet}} < 1$	$\sigma_{\text{eff}} \sim 5$ mb
UA2, 1991 [19]	630	4 jets	$p_T^{\text{jet}} > 15$	$ \eta^{\text{jet}} < 2$	$\sigma_{\text{eff}} > 8.3$ mb (95% C.L.)
CDF, 1993 [20]	1800	4 jets	$p_T^{\text{jet}} > 25$	$ \eta^{\text{jet}} < 3.5$	$\sigma_{\text{eff}} = 12.1^{+10.7}_{-5.4}$ mb
D0, 2014 [25]	1960	$J/\psi J/\psi$	$p_T^{J/\psi} > 4$	$ \eta^{J/\psi} < 2.2$	$\sigma_{\text{eff}} = 4.8 \pm 0.5 \pm 2.5$ mb
LHCb, 2015 [27]	7000, 8000	ΥD^{0+}	$p_T^{\Upsilon} < 15$	$2.0 < y^{\Upsilon} < 4.5$	$\sigma_{\text{eff}} = 18 \pm 1.8$ mb
D0, 2015 [26]	1960	$J/\psi \Upsilon$	$p_T^{\Upsilon} > 2$	$ \eta^{\Upsilon} < 2$	$\sigma_{\text{eff}} = 2.2 \pm 0.7 \pm 0.9$ mb
CDF, 1997 [21]	1800	$\gamma + 3$ jets	$p_T^{\text{jet}} > 6$ $p_T^{\gamma} > 16$	$ \eta^{\text{jet}} < 3.5$ $ \eta^{\gamma} < 0.9$	$\sigma_{\text{eff}} = 14.5 \pm 1.7^{+1.7}_{-2.3}$ mb
D0, 2009 [22]	1960	$\gamma + 3$ jets	$60 < p_T^{\gamma} < 80$	$ \eta^{\gamma} < 1.0$ $1.5 < \eta^{\gamma} < 2.5$	$\sigma_{\text{eff}} = 16.4 \pm 2.3$ mb
D0, 2014 [24]	1960	$\gamma + 3$ jets	$p_T^{\gamma} > 26$	$ \eta^{\gamma} < 1.0$ $1.5 < \eta^{\gamma} < 2.5$	$\sigma_{\text{eff}} = 12.7 \pm 1.3$ mb
D0, 2014 [24]	1960	$\gamma + b/c$ jet + 2 jets	$p_T^{\gamma} > 26$	$ \eta^{\gamma} < 1.0$ $1.5 < \eta^{\gamma} < 2.5$	$\sigma_{\text{eff}} = 14.6 \pm 3.3$ mb
ATLAS, 2013 [28]	7000	$W + 2$ jets	$p_T^{\text{jet}} > 20$	$ \eta^{\text{jet}} < 2.8$	$\sigma_{\text{eff}} = 15 \pm 3^{+5}_{-3}$ mb
CMS, 2014 [29]	7000	$W + 2$ jets	$p_T^{\text{jet}} > 20$	$ \eta^{\text{jet}} < 2.0$	$\sigma_{\text{eff}} = 20.7 \pm 6.6$ mb

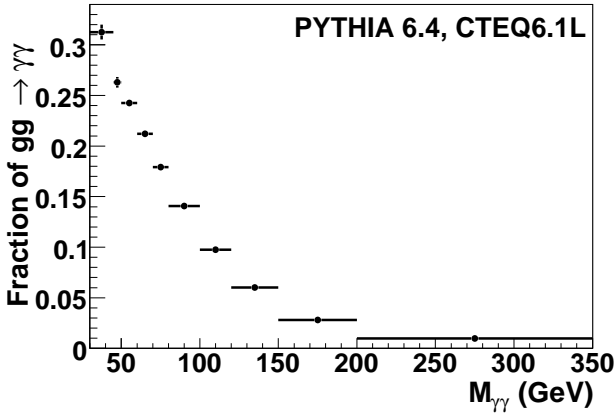


FIG. 2: Fraction of the $gg \rightarrow \gamma\gamma$ contribution to the total direct cross section comprising the $q\bar{q} \rightarrow \gamma\gamma$ and $gg \rightarrow \gamma\gamma$ processes. $M_{\gamma\gamma}$ is the invariant mass of the diphoton.

ter class of events, referred to as double interaction (DI) events, two hard parton interactions occur in exactly two separate $p\bar{p}$ collisions within the same beam crossing.

The single [33, 34] and double [35] diffractive processes contribute approximately 1% to the total dijet production cross section with jet $p_T \gtrsim 15$ GeV. Therefore, the diphoton and dijet events are produced mainly as a result of inelastic nondiffractive (hard) $p\bar{p}$ interactions. In a $p\bar{p}$ beam crossing with two inelastic nondiffractive collisions the probability for a DI event is

$$P_{\text{DI}} = 2 \frac{\sigma^{\gamma\gamma}}{\sigma_{\text{hard}}} \frac{\sigma^{jj}}{\sigma_{\text{hard}}}, \quad (3)$$

where $\sigma^{\gamma\gamma}/\sigma_{\text{hard}}$ ($\sigma^{jj}/\sigma_{\text{hard}}$) is the probability for producing a diphoton (dijet) event satisfying particular photon (jet) selection criteria in two separate hard processes and σ_{hard} is the cross section of the hard $p\bar{p}$ interactions. The factor of 2 accounts for the fact that the two scatterings (producing diphoton and dijet events) can be ordered in two ways with respect to the two collision vertices. The number of DI events can be obtained from P_{DI} , after correcting for geometric and kinematic acceptance A_{DI} , selection efficiency (including trigger efficiency) ϵ_{DI} , and the two-vertex selection efficiency $\epsilon_{2\text{vtx}}$ and multiplying by the number of beam crossings with exactly two hard collisions $N_c(2)$:

$$N_{\text{DI}} = 2 \frac{\sigma^{\gamma\gamma}}{\sigma_{\text{hard}}} \frac{\sigma^{jj}}{\sigma_{\text{hard}}} N_c(2) A_{\text{DI}} \epsilon_{\text{DI}} \epsilon_{2\text{vtx}}. \quad (4)$$

Similarly to P_{DI} , the probability for DP events, P_{DP} , in a beam crossing with one hard collision, using Eq. (2), is,

$$P_{\text{DP}} = \frac{\sigma^{\text{DP}}}{\sigma_{\text{hard}}} = \frac{\sigma^{\gamma\gamma}}{\sigma_{\text{eff}}} \frac{\sigma^{jj}}{\sigma_{\text{hard}}}. \quad (5)$$

The parton scatterings in the DP events are assumed to be uncorrelated [1–9]. The number of DP events, N_{DP} , can be expressed as P_{DP} corrected for the acceptance A_{DP} , selection efficiency (including trigger efficiency) ϵ_{DP} , and the single vertex selection efficiency $\epsilon_{1\text{vtx}}$, multiplied by the number of beam crossings with exactly one hard collision $N_c(1)$:

$$N_{\text{DP}} = \frac{\sigma^{\gamma\gamma}}{\sigma_{\text{eff}}} \frac{\sigma^{jj}}{\sigma_{\text{hard}}} N_c(1) A_{\text{DP}} \epsilon_{\text{DP}} \epsilon_{1\text{vtx}}. \quad (6)$$

Taking the ratio $N_{\text{DI}}/N_{\text{DP}}$ allows one to obtain an expression for σ_{eff} ,

$$\sigma_{\text{eff}} = \frac{N_{\text{DI}}}{N_{\text{DP}}} \frac{A_{\text{DP}}}{A_{\text{DI}}} \frac{\epsilon_{\text{DP}}}{\epsilon_{\text{DI}}} \frac{\epsilon_{1\text{vtx}}}{\epsilon_{2\text{vtx}}} R_c \sigma_{\text{hard}}, \quad (7)$$

where $R_c = N_c(1)/2N_c(2)$.

It is worth noting that (a) the $\sigma^{\gamma\gamma}$ and σ^{jj} cross sections cancel in this ratio and (b) the efficiencies and acceptances for DP and DI events enter only as ratios (i.e. all common uncertainties are reduced as well). To calculate these efficiencies, acceptances, and their ratios, we use the data based models which are described in Sec. IV A.

The numbers of DI (DP) events N_{DI} (N_{DP}) can be determined from the number of two- (one-)vertex $\gamma\gamma$ + dijet events $N_{2\text{vtx}}$ ($N_{1\text{vtx}}$) as $N_{\text{DI}} = f_{\text{DI}} P_{\text{DI}}^{\gamma\gamma} N_{2\text{vtx}}$ ($N_{\text{DP}} = f_{\text{DP}} P_{\text{DP}}^{\gamma\gamma} N_{1\text{vtx}}$), where f_{DI} (f_{DP}) and $P_{\text{DI}}^{\gamma\gamma}$ ($P_{\text{DP}}^{\gamma\gamma}$) are the fraction of DI (DP) events and diphoton purity in the two- (one-)vertex data set, respectively. The fraction f_{DP} is estimated from the data set with one $p\bar{p}$ collision using a fraction ratio method, while f_{DI} can be obtained from data events with two $p\bar{p}$ collisions using a jet-track algorithm. The complete description of the techniques used for f_{DP} and f_{DI} estimates are described in Secs. VIA and VIB, and the diphoton sample purity is discussed in Sec. VII A.

The main background for the DP events is due to contributions from the SP scattering processes, $q\bar{q} \rightarrow \gamma\gamma gg$, and $gg \rightarrow \gamma\gamma gg$. These processes mainly result from gluon radiation in the initial or the final state and can also result from photon fragmentation events.

III. D0 DETECTOR AND DATA SAMPLES

The D0 detector is described in detail in Refs. [36–38]. Photon candidates are identified as isolated clusters of energy depositions in one of three uranium and liquid argon sampling calorimeters. The central calorimeter covers the pseudorapidity range $|\eta_{\text{det}}| < 1.1$, and the two end calorimeters extend the coverage up to $|\eta_{\text{det}}| \approx 4.2$. In addition, the plastic scintillator intercryostat detector covers the region $1.1 < |\eta_{\text{det}}| < 1.4$. The electromagnetic (EM) section of the calorimeter is segmented longitudinally into four layers and transversely into cells in pseudorapidity and azimuthal angle $\Delta\eta_{\text{det}} \times \Delta\phi_{\text{det}} = 0.1 \times 0.1$ (0.05×0.05 in the third layer of the EM calorimeter). The hadronic portion of the calorimeter is located behind the EM section. The calorimeter surrounds a tracking system consisting of a silicon microstrip tracking detector and scintillating fiber tracker, both located within a 1.9 T solenoidal magnetic field. The solenoid magnet is surrounded by the central preshower (CPS) detector located immediately before the calorimeter. The CPS consists of approximately one radiation length of lead absorber at normal incidence surrounded by three layers of scintillating strips. The luminosity of colliding beams is measured using plastic scintillator arrays installed in front of the two end calorimeter cryostats [39].

The current measurement is based on 8.7 fb^{-1} of data collected using $p\bar{p}$ collisions at $\sqrt{s} = 1.96 \text{ TeV}$ after the D0 detector upgrade in 2006 [38], while the previous measurements [22, 23] were made using the data collected before this upgrade. The events used in this analysis pass the triggers designed to identify high- p_T clusters in the EM calorimeter with loose shower shape requirements for photons. These triggers have $\approx 90\%$ efficiency for a photon transverse momentum $p_T^\gamma \approx 16 \text{ GeV}$ and are 100% efficient for $p_T^\gamma > 35 \text{ GeV}$.

To select photon candidates in our data samples, we use the following criteria [40, 41]: EM objects are reconstructed using a simple cone algorithm with a cone size of $\Delta\mathcal{R} = \sqrt{(\Delta\eta)^2 + (\Delta\phi)^2} = 0.2$. Regions with poor photon identification and degraded p_T^γ resolution at the boundaries between calorimeter modules and between the central and end cap calorimeters are excluded from the analysis. Each photon candidate is required to deposit more than 96% of the detected energy in the EM section of the calorimeter and to be isolated in the angular region between $\Delta\mathcal{R} = 0.2$ and $\Delta\mathcal{R} = 0.4$ around the center of the cluster: $(E_{\text{tot}}^{\text{iso}} - E_{\text{core}}^{\text{iso}})/E_{\text{core}}^{\text{iso}} < 0.07$, where $E_{\text{tot}}^{\text{iso}}$ is the total (EM+hadronic) tower energy in the (η, ϕ) cone of radius $\Delta\mathcal{R} = 0.4$ and $E_{\text{core}}^{\text{iso}}$ is EM energy within a radius of $\Delta\mathcal{R} = 0.2$. Candidate EM clusters that match to a reconstructed track are excluded from the analysis. We also require the energy-weighted EM cluster width in the finely segmented third EM layer to be consistent with that expected for a photon-initiated electromagnetic shower. In addition to the calorimeter isolation cut, we also apply a track isolation cut, requiring the scalar sum of the track transverse momenta in an annulus $0.05 \leq \Delta\mathcal{R} \leq 0.4$ to be less than 1.5 GeV. To further suppress the jet background, the photons are selected to satisfy the same requirement on a neural network (NN) discriminant as in Ref. [42].

Jets are reconstructed using an iterative midpoint cone algorithm [43] with a cone size of 0.7. Jets must satisfy quality criteria that suppress background from leptons, photons, and detector noise effects. Jet transverse momenta are corrected to the particle level [44].

Two photons must be separated from each other by $\Delta\mathcal{R} > 0.4$ and from each jet by $\Delta\mathcal{R} > 0.9$. Jets must be separated from each other by $\Delta\mathcal{R} > 1.4$. Each event must contain at least two photons in the pseudorapidity region $|\eta^\gamma| < 1.0$ and at least two jets with $|\eta^{\text{jet}}| < 3.5$. The photon with the highest p_T is named the “leading photon,” or first photon, and the photon with the second highest p_T is denoted as the second photon. Similar terminology is applied to the jets. Events are selected with the leading photon transverse momentum $p_T^\gamma > 16 \text{ GeV}$, the second photon $p_T^\gamma > 15 \text{ GeV}$, and jets satisfying $15 < p_T^{\text{jet}} < 40 \text{ GeV}$. The upper requirement on the p_T of the jets increases the fraction of DP events in the sample [22]. The numbers of events with exactly one identified $p\bar{p}$ collision (1VTX), exactly two identified $p\bar{p}$ collisions (2VTX), and their ratio are shown in Table II. The $p\bar{p}$ collision vertices are reconstructed using a

track-based algorithm and are sorted according to their tracking activity. The vertices are required to be within $|z| < 60$ cm from the geometric center of the detector (the detector luminous region rms is ~ 20 cm) and have $N_{trk} \geq 3$ tracks. The vertex at the top of the list (PV0) and the second-best (PV1) vertex have the highest and the second-highest tracking multiplicities, respectively.

TABLE II: The number of selected $\gamma\gamma$ + dijet events with a single $p\bar{p}$ collision (N_{1vtx}), two $p\bar{p}$ collisions (N_{2vtx}), and their ratio.

N_{1vtx}	N_{2vtx}	N_{2vtx}/N_{1vtx}
401	442	1.102

IV. DATA, SIGNAL, AND BACKGROUND EVENT MODELS

This section presents an overview of the DP and DI models built using data and Monte-Carlo (MC) samples to estimate the number of DP and DI events in data, N_{DP} and N_{DI} . These models are also used to estimate the selection efficiencies and geometric and kinematic acceptances for DP and DI events.

A. Signal models

Because σ_{eff} depends on DP and DI events as shown in Eq. (7), both classes of events are considered signal events:

- (i) DP data event model (MIXDP): The DP event model is constructed by combining photons and jets from two events drawn from two samples: (a) an inclusive data sample of $\gamma\gamma$ events and (b) a sample of inelastic nondiffractive events selected with a minimum bias trigger (a trigger that only requires hits in the luminosity detectors) and a requirement of at least one reconstructed jet (“MB” sample) [22, 44]. Both input samples contain events with exactly one reconstructed $p\bar{p}$ collision vertex. The resulting mixed event is required to satisfy the same selection criteria as applied to $\gamma\gamma$ + dijet data events with a single $p\bar{p}$ collision. By construction, the MIXDP sample provides independent parton scatterings with $\gamma\gamma$ and dijet final states. Because the $\gamma\gamma$ process in a DP event is dominated by small parton momentum fractions (x), the x values in the dijet production process remaining after the first parton interaction occurs are expected to be generally unaffected; i.e., the two interactions have negligible correlation in momentum space. We have verified that the effect of adding the diphoton and dijet components in MIXDP with different vertex positions is negligible, since the MIXDP model is

only used for modelling the transverse discriminating variable introduced below in Sec. V. Two possible event configurations with the $\gamma\gamma$ + dijet final state in a single $p\bar{p}$ collision are shown in Fig. 3.

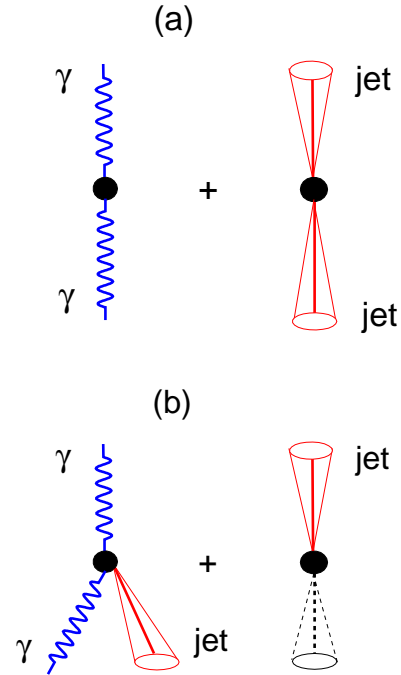


FIG. 3: Diagrams of $\gamma\gamma$ + dijet final state in the events with a single $p\bar{p}$ collision. (a) DP scattering with diphoton production overlaid with dijet production; (b) DP scattering with diphoton +1 jet production overlaid with dijet production, in which one of the two jets is lost (dotted line). They can also be used as an illustration of the two DI events if one assumes that the processes shown come from two distinct $p\bar{p}$ collisions.

- (ii) DI data event model (MIXDPI): The $\gamma\gamma$ + dijet DI signal event model is built from an overlay of $\gamma\gamma$ and MB events with ≥ 1 selected jets. This sample is prepared similarly to the MIXDP sample but with the requirement of exactly two reconstructed $p\bar{p}$ collision vertices in both data samples instead of one such vertex in the samples used for MIXDP. Thus, the second $p\bar{p}$ collision contains only soft underlying energy that can contribute energy to a jet cone, or a photon isolation cone. In addition, in the case of jets in the MB component of the MIXDPI mixture, if there is more than one jet, both jets are required to originate from the same vertex, using jet-track information, as discussed in Appendix B of Ref. [22]. The resulting $\gamma\gamma$ + dijet events undergo the same selection as applied to the data sample with two $p\bar{p}$ collision vertices.
- (iii) DP and DI MC models (MCDP and MCDI): To create signal MC models for DP and DI events, we use an overlay of MC $\gamma\gamma$ and dijet events. These events are generated with the SHERPA [45] and PYTHIA [46]

event generators, respectively, and are processed by a GEANT-based [47] simulation of the D0 detector response. To accurately model the effects of multiple $p\bar{p}$ interactions and detector noise, data events from random $p\bar{p}$ crossings are overlaid on the MC events using data from the same data taking period as considered in the analysis. These MC events are then processed using the same reconstruction software as for data. We also apply additional smearing to the reconstructed photon and jet p_T so that the measurement resolutions in MC match those in the data. These MC events are used to create single- and two-vertex samples.

Using the $\gamma\gamma$ and dijet MC samples, we create $\gamma\gamma$ +dijet DP and DI MC models, similarly to those constructed for MIXDP and MIXDPI data samples, i.e., with only one and only two reconstructed primary interaction vertexes, respectively, by examining information for jets and the photon at both the reconstructed and particle level. These samples are used to calculate selection efficiencies and acceptances for DP and DI events. As a cross check, we have compared the p_T and η distributions of the jets and photons at the reconstructed level in these models with those in the MIXDP and MIXDPI data samples. Small discrepancies have been resolved by reweighting these MC spectra and creating models denoted as datalike MCDP and MCDI.

B. Background model

To extract the DP signal from the data, we need to subtract $\gamma\gamma$ +dijet SP background.

- (i) SP one-vertex event model (SP1VTX): A background to the DP events arises predominantly from $\gamma\gamma$ production with two jets, resulting in a $\gamma\gamma$ + dijet final state in a single $p\bar{p}$ collision event. To model this background, we consider a sample of MC $\gamma\gamma$ +dijet events generated with PYTHIA and SHERPA with multiple parton interaction modeling turned off. The SP1VTX sample contains the final state with two photons and two additional jets with the same selection criteria as applied to the data sample with a single $p\bar{p}$ collision vertex. Other small backgrounds are included in the event generators. The SHERPA SP model is taken as the default.

V. DISCRIMINATING VARIABLE

A DP event contains two independent $2 \rightarrow 2$ parton-parton scatterings within the same $p\bar{p}$ collision. The same final state can be produced by the SP $2 \rightarrow 4$ process, resulting in $\gamma\gamma$ and two bremsstrahlung jets with substantially different kinematic distributions. Discrimination between these processes is obtained by exploiting

the azimuthal angle between the p_T imbalance vectors of photon and jet pairs in $\gamma\gamma$ + dijet events,

$$\Delta S \equiv \Delta\phi(\vec{q}_T^1, \vec{q}_T^2), \quad (8)$$

where $\vec{q}_T^1 = \vec{p}_T^{\gamma 1} + \vec{p}_T^{\gamma 2}$ and $\vec{q}_T^2 = \vec{p}_T^{\text{jet}1} + \vec{p}_T^{\text{jet}2}$. Figure 4 illustrates the orientation of photons and jets transverse momentum vectors in $\gamma\gamma$ + dijet events, as well as the imbalance vectors \vec{q}_T^1 and \vec{q}_T^2 .

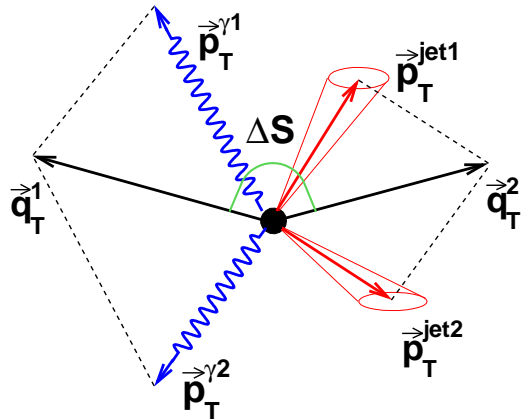


FIG. 4: A diagram illustrating the orientation of photon and jet transverse momenta vectors in $\gamma\gamma$ + dijet events. Vectors q_T^1 and q_T^2 are the p_T imbalance vectors of diphoton and dijet pairs, respectively.

For DP events in which the photons come from one parton-parton scattering and the two jets come from another parton-parton scattering, the ΔS angle is isotropically distributed. However, the DP events with an additional bremsstrahlung jet in the first parton-parton scattering shown in Fig. 3(b) tend to populate the region toward $\Delta S = \pi$ due to momentum conservation. The bremsstrahlung processes also cause ΔS to peak strongly near π in SP, but detector resolution effects and gluon radiation in parton showers produce a tail extending to smaller angles.

VI. FRACTIONS OF DP AND DI EVENTS

A. Fractions of DP events

In order to calculate σ_{eff} , one needs to measure the number of DP events (N_{DP}) which enters Eq. (7), as the product of the fraction of DP events (f_{DP}) in the 1VTX data sample, the size of the 1VTX sample, and its diphoton purity. The fraction is estimated in the $\gamma\gamma$ + dijet 1VTX data sample using the MIXDP and the SP1VTX models described in Sec. IV.

The observed number of data events, N_{data}^n , with ΔS less than a cut ΔS^n can be written as

$$N_{\text{data}}^n = f_{\text{DP}}^n N_{\text{DP}}^n + (1 - f_{\text{DP}}^n) N_{\text{SP}}^n,$$

where the number of DP events normalized to the data sample is $N_{\text{DP}}^n = (N_{\text{data}}^{\text{tot}}/M_{\text{DP}}^{\text{tot}})M_{\text{DP}}^n$, $N_{\text{data}}^{\text{tot}}$ and $M_{\text{DP}}^{\text{tot}}$ are the total number of events in the data and MIXDP samples for all values of ΔS , and M_{DP}^n is the number of MIXDP events below the cut ΔS^n . A similar construction is used to define N_{SP}^n using the SP1VTX sample. We define the fractions $\epsilon_{\text{data}}^n = N_{\text{data}}^n/N_{\text{data}}^{\text{tot}}$, $\epsilon_{\text{DP}}^n = N_{\text{DP}}^n/N_{\text{DP}}^{\text{tot}}$, and $\epsilon_{\text{SP}}^n = N_{\text{SP}}^n/N_{\text{SP}}^{\text{tot}}$ and use the fact that $N_{\text{DP}}^{\text{tot}} = N_{\text{SP}}^{\text{tot}} = N_{\text{data}}^{\text{tot}}$ to obtain

$$\epsilon_{\text{data}}^n = f_{\text{DP}}^n \epsilon_{\text{DP}}^n + (1 - f_{\text{DP}}^n) \epsilon_{\text{SP}}^n,$$

which yields

$$f_{\text{DP}}^n = \frac{\epsilon_{\text{data}}^n - \epsilon_{\text{SP}}^n}{\epsilon_{\text{DP}}^n - \epsilon_{\text{SP}}^n}. \quad (9)$$

Due to the definitions of the fractions ϵ^n , this expression for f_{DP}^n depends upon the numbers of events in the data, DP, and SP distributions both below and above the cut, ΔS^n . To estimate the uncertainties in the shapes of the M_{DP} and M_{SP} distributions of MIXDP and SP1VTX events, respectively, as a function of ΔS , we compute f_{DP}^n for seven different values of the cut value ΔS^n , and average the results, taking into account the correlations in the numbers of events in the different samples. We also estimate the uncertainty due to model dependence of the SP1VTX sample as in the appendix of Ref. [24] by reweighting the models to data, based on the kinematic distribution $\Delta\phi(\gamma, \gamma)$ and the jet p_T spectra. The differences between estimates made with the original and the modified models are included in the systematic uncertainty. The background due to DP photon-3jet events is corrected for using the diphoton purity estimate; see Sec. VII A. Using an inclusive $\gamma + \text{jet}$ sample [40], we estimate the fraction of DP $\gamma + \text{jet}$ events to be less than 2.0%. We do not correct for this effect and include the entire estimate of the contamination as a systematic uncertainty. Finally, we get

$$f_{\text{DP}}^{\text{avg}} = 0.213 \pm 0.061(\text{stat}) \pm 0.028(\text{syst}). \quad (10)$$

As a cross check, the fraction f_{DP} is found using a maximum likelihood fit [48] of the ΔS distribution of the data to signal and background templates that are taken to be the shapes of M_{DP} and M_{SP} , respectively. Signal and background models are described in Sec. IV and undergo all the selection criteria applied to the data sample. From the fit we find a f_{DP} value of 0.18 ± 0.11 , which agrees with the value estimated by the average fraction method within uncertainty. The result of the fit is shown in Fig. 5.

B. Fractions of DI events

Double interaction events in the 2VTX sample arising from different $p\bar{p}$ interactions within the same bunch crossing include those events in which the $\gamma\gamma$ and dijets

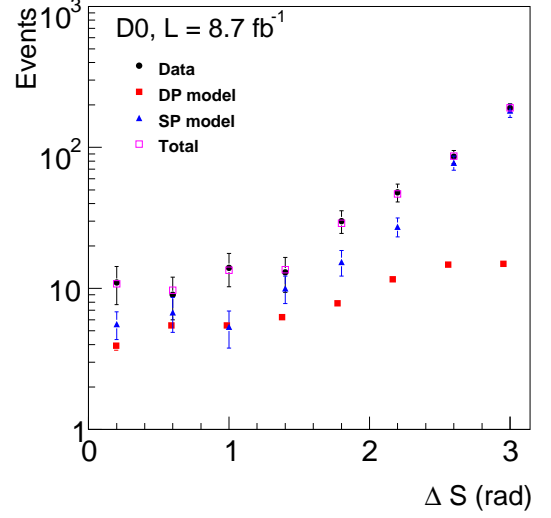


FIG. 5: The fit of the 1VTX data ΔS distribution with SP and DP templates to extract the DP fraction. The black points correspond to data, red boxes to the DP signal MIXDP model normalized to the f_{DP} fraction obtained from the fit, and the blue triangles are the SP background template (SP1VTX) normalized to its fraction $(1 - f_{\text{DP}})$. The pink open boxes correspond to the sum of the signal and background (total).

are associated with different vertices and those in which the two jets are associated with different vertices irrespective of the photons' vertex associations. Backgrounds to the DI events in the two-vertex sample come from those events in which the two photons and the two jets are associated with the same vertex (and there is an additional MB vertex containing neither a γ nor jet). The DI fraction, f_{DI} , is defined as the ratio of the number of DI events to the sum of the DI and background events.

The vertex association for jets is based on the p_T -weighted average, $\langle z_{\text{vtx}} \rangle$, of the z positions (points of the closest approach to z axis) of all tracks associated with the jet and the charged particle fraction (CPF) discriminant that measures the fraction of the total charged particle p_T in each jet i that is associated with vertex j ,

$$\text{CPF}(\text{jet}_i, \text{vtx}_j) = \frac{\sum_k p_T(\text{trk}_k^{\text{jet}_i}, \text{vtx}_j)}{\sum_n \sum_l p_T(\text{trk}_l^{\text{jet}_i}, \text{vtx}_n)}, \quad (11)$$

where the sum is taken over tracks within the jet cone in the numerator and also over all vertices in the denominator. For the calculation of f_{DI} , we require each jet to contain at least two tracks and to satisfy $\text{CPF} > 0.65$ for one of the two vertices. Using a sample of $\gamma + \text{jet}$ events with exactly one observed vertex, we find the resolution in the p_T -weighted jet z position to be $\sigma_z^{\text{jet}} = 1.2$ cm. We require a valid jet to point to one of the vertices within $3\sigma_z^{\text{jet}}$.

The z -resolution of photons using only the information from the EM calorimeter is too coarse to be of use in making a vertex association. However, for those pho-

tons in which there is a good three-dimensional cluster seen in the CPS, the combined EM calorimeter and CPS position information provides a photon pointing resolution of $\sigma_z^\gamma = 3$ cm. We require a CPS tagged photon to point to one of the vertices within $3\sigma_z^\gamma$.

The fraction of events in the total DI sample of 442 events (cf. Table II) in which the two jets are associated with different vertices is 14.6%. In this estimate, no requirement on the photon vertex assignments is made. Using an inclusive γ +jet sample [40], we estimate the fraction of non-DI events in which a γ +jet is associated with each of the different vertices to be less than 0.5%.

About one-quarter of all two-vertex events have CPS pointing information for both photons. Using this sample, we estimate that 4.7% of the two-vertex events are DI events in which the diphotons are associated with one vertex and the dijet systems are associated with the other. Due to the small sample statistics and relatively large σ_z^γ , we assign a 50% uncertainty on this component of f_{DI} . Taking the two categories of DI events together, we find $f_{\text{DI}} = 0.193 \pm 0.021(\text{stat}) \pm 0.028(\text{syst})$.

The DI fraction could depend on the distance in z between the two vertices. To study this effect, the distance between the two vertices is varied up to $7\sigma_z^{\text{jet}}$, and the DI fraction is extracted with the requirement above. Table III shows f_{DI} with respect to the distance between two vertices, $\Delta z(PV0, PV1)$. The difference between the default f_{DI} value and f_{DI} found when the distance between the two vertices is greater than $7\sigma_z^{\text{jet}}$ is added to the systematic uncertainty. The default choice corresponds to no restriction on $\Delta z(PV0, PV1)$. Finally, the DI fraction

TABLE III: DI event fraction with respect to $\Delta z(PV0, PV1)$.

$\Delta z(PV0, PV1)$	f_{DI}
Default	$0.193 \pm 0.021(\text{stat}) \pm 0.028(\text{syst})$
$> 3\sigma_z^{\text{jet}}$	$0.195 \pm 0.021(\text{stat}) \pm 0.028(\text{syst})$
$> 5\sigma_z^{\text{jet}}$	$0.200 \pm 0.022(\text{stat}) \pm 0.028(\text{syst})$
$> 7\sigma_z^{\text{jet}}$	$0.203 \pm 0.023(\text{stat}) \pm 0.028(\text{syst})$

extracted is:

$$f_{\text{DI}} = 0.193 \pm 0.021 (\text{stat}) \pm 0.030 (\text{syst}) \quad (12)$$

VII. DP AND DI EFFICIENCIES, R_c AND σ_{hard}

A. Ratio of photon purity in DP and DI events

As mentioned in Sec. II, the numbers of events N_{DI} and N_{DP} in Eq. (7) depend on the purity of the diphoton sample. There are two major sources of background events to direct diphoton production: (i) Drell-Yan (DY) events with both electrons misidentified as photons due to tracking inefficiency and (ii) γ +jet and dijet events with jet(s) misidentified as photon(s) [42]. The W +jet/ γ background with $W \rightarrow e\nu$ decay has been estimated from MC and is found to be negligible. The number of data

events that satisfy the photon selection criteria can be written as the sum of true diphoton events, DY events and γ +jet or dijet events that fake the two photon signature.

We use $Z/\gamma^* \rightarrow ee$ PYTHIA+ALPGEN MC samples to estimate the DY contribution. The next-to-next-to-leading-order $p\bar{p} \rightarrow Z/\gamma^* \rightarrow ee$ cross section [49] is used for the absolute normalization and the generator level Z/γ^* boson p_T has been reweighted to the measured data distribution. The expected number of events from the DY process is 2.19(0.5%) and 2.41(0.5%) in case of 1VTX and 2VTX events, respectively. The numbers in parentheses correspond to the percentage of the DY contribution to the data sample.

To estimate the fraction of diphoton events, we use variables sensitive to the internal structure of the electromagnetic shower. The outputs of the photon NN [42] for the photons in the central calorimeter, trained on MC samples with direct photons and dijets, have been chosen as a discriminant between signal and background events. Since the signal events cannot be identified on an event by event basis, their fraction (purity) $P^{\gamma\gamma}$, defined as the ratio of the number of two photon events to the total number of candidate events satisfying the selection criteria, is determined statistically.

The two-dimensional distribution of NN outputs of the two photon candidates in data after subtracting the DY contribution is fitted using two-dimensional NN output templates of signal photons from the SHERPA and PYTHIA MC and templates of jets from PYTHIA MC jet samples, where special requirements are applied at the generator level to enrich the sample with jets having an electromagnetic shower shape similar to that of the photon [42]. The fit uses the same maximum likelihood method [48] as for the cross check fit for f_{DP} ; see Sec. VIA. The results of the diphoton purities in DP and DI events and their ratio are presented in Table IV.

TABLE IV: Diphoton event purity in DP and DI events and their ratio. The uncertainties are statistical.

Sample	SHERPA	PYTHIA
$P_{\text{DP}}^{\gamma\gamma}$	0.688 ± 0.005	0.608 ± 0.028
$P_{\text{DI}}^{\gamma\gamma}$	0.689 ± 0.025	0.623 ± 0.029
$P_{\text{DI}}^{\gamma\gamma}/P_{\text{DP}}^{\gamma\gamma}$	1.002 ± 0.039	1.025 ± 0.067

We identify an additional source of systematic uncertainty due to model dependence as half of the difference between the ratio of purities calculated using different signal models generated by PYTHIA and SHERPA. It is estimated to be 1.2%.

Another source of systematic uncertainty is due to the fragmentation model used in PYTHIA and caused by the uncertainty in the fragmentation functions $D_{\pi,\eta}(z)$. This uncertainty is estimated by varying the number of π^0 and η mesons in the dijet sample by a factor of 2 and calculating the purity using the modified templates. It is

found to be equal to 3%.

B. Ratio of geometric acceptance times efficiency in DP and DI events

The acceptance (A) is calculated as a ratio of $N_i^{\text{reco}}/N_i^{\text{gen}}$, where N_i^{reco} and N_i^{gen} are the numbers of simulated events at the reconstruction and generator (true) level, respectively. It accounts for events lost during event reconstruction, for objects created by spurious hits, and the contribution from true objects outside the fiducial region but reconstructed inside the fiducial region and vice versa.

To estimate acceptances in one and two $p\bar{p}$ collision samples, we use the signal MCDP and MCDI samples described in Sec. IV. These samples mix diphoton events generated by SHERPA and dijet events generated by PYTHIA. The acceptance is calculated using the following photon and jet selection criteria:

(1) Generator level:

(a) $p_T^{\gamma_1} > 16$ GeV, $p_T^{\gamma_2} > 15$ GeV, $|\eta| < 1.0$;

(b) jets with $15 < p_T^{\text{jet}} \leq 40$ GeV and $|\eta^{\text{jet}}| < 3.5$;

(2) Reconstruction level:

(a) $p_T^{\gamma_1} > 16$ GeV, $p_T^{\gamma_2} > 15$ GeV, $|\eta| < 1.0$, $|\eta^{\text{det}}| < 1.0$;

photon candidates are required to be away from the calorimeter module boundaries in ϕ^{det} ; the fraction of the photon energy in the EM calorimeter is required to be greater than 0.9; and the fraction of energy in the calorimeter isolation annulus $0.2 < \Delta R < 0.4$ around the photon is required to be 0.15 of that within the $\Delta R = 0.2$ cone;

(b) jets with $15 < p_T^{\text{jet}} \leq 40$ GeV, $|\eta^{\text{jet}}| < 3.5$.

In Table V, we present the photon and jet acceptance for 1VTX (MCDP) and 2VTX (MCDI) samples and their ratio. The difference between 1VTX and 2VTX accep-

TABLE V: Geometric acceptances in DP and DI events and their ratio.

A_{DP}	A_{DI}	$A_{\text{DP}}/A_{\text{DI}}$
0.429 ± 0.008	0.826 ± 0.019	0.521 ± 0.015

tances is mostly caused by different amounts of underlying energy falling inside the photon and jet cones, resulting in different efficiencies for passing the photon and jet p_T requirements. The uncertainties due to the jet energy scale (JES) and the model dependence of the individual acceptances largely cancel in the ratio.

C. Ratio of photon efficiencies in DP and DI events

The DP and DI events differ from each other by the number of $p\bar{p}$ collision vertices (one vs. two), and therefore their selection efficiencies ϵ_{DP} and ϵ_{DI} may differ due to different amounts of soft unclustered energy in the single and double $p\bar{p}$ collision events. This could lead to different photon selection efficiencies because of different distortions of the shower shape that this unclustered energy may introduce into the track and calorimeter isolation cones around the photon.

The efficiency for passing the photon selection criteria is estimated using $\gamma\gamma$ + dijet PYTHIA and SHERPA MC events. The events are preselected with all jet cuts and loose photon identification cuts (as used in the acceptance calculation), and 1VTX and 2VTX samples are extracted from them. The efficiency is calculated from the ratio of the number of events that pass the photon selection criteria, weighted by the trigger efficiency to the number of events that pass the preselection criteria. In Table VI, we present the photon efficiencies for DP and DI events. Uncertainties are due to limited MC statistics.

TABLE VI: Photon efficiencies in single and double $p\bar{p}$ collisions $\gamma\gamma$ + dijet SHERPA and PYTHIA MC samples. Uncertainties are due to limited MC statistics.

Sample	SHERPA	PYTHIA
ϵ_{DP}	0.477 ± 0.035	0.576 ± 0.010
ϵ_{DI}	0.333 ± 0.021	0.419 ± 0.009
$\epsilon_{\text{DP}}/\epsilon_{\text{DI}}$	1.434 ± 0.138	1.372 ± 0.039

The difference in the efficiencies between PYTHIA and SHERPA is used as an estimate of the systematic uncertainty due to model dependence. The selection efficiencies for DP and DI events enter Eq. (7) only as a ratio, substantially canceling correlated systematic uncertainties. The PYTHIA ratio, which has a smaller statistical uncertainty, is used in the σ_{eff} calculation.

D. Ratio of vertex efficiencies

An efficiency, $\epsilon_{1\text{vtx}}$ ($\epsilon_{2\text{vtx}}$), calculated for the DP (DI) candidate samples, is mostly due to the single (double) vertex requirements, $|z| < 60$ cm and $N_{\text{trk}} \geq 3$. The contribution of the vertex reconstruction efficiency to this quantity is partially absorbed into the acceptance calculation and very close to unity, as we discuss below. To calculate the efficiency for events with 1 $p\bar{p}$ collision to pass the vertex requirement, we use the $\gamma\gamma$ + dijet data with photon and jet selection criteria. The efficiency for simultaneously satisfying the two-vertex requirement is estimated separately for each jet-vertex assignment configuration, since the vertex efficiency depends on the objects originating from the vertex. For diphoton-dijet events originating from two separate vertices, we calculate $\epsilon_{2\text{vtx}}$

as a product of the efficiency to pass the vertex cuts in the diphoton 2VTX data sample and the efficiency to pass the vertex cuts for dijets in the 2VTX MB sample. Similarly, for events with two jets originating from two separate vertices, we calculate the $\epsilon_{2\text{vtx}}$ efficiency as a product of the efficiency to pass the vertex cuts for the $\gamma\gamma + 1$ jet 2VTX data sample and the efficiency to pass the vertex cuts for jets in the 2VTX MB sample. The final efficiency is a combination of the two, weighted by the event-type fraction. Table VII presents the vertex efficiencies for 1VTX and 2VTX samples and their ratio.

TABLE VII: Vertex efficiencies for 1VTX and 2VTX samples and their ratio.

$\epsilon_{1\text{vtx}}$	$\epsilon_{2\text{vtx}}$	$\epsilon_{1\text{vtx}}/\epsilon_{2\text{vtx}}$
0.944 ± 0.003	0.922 ± 0.003	1.021 ± 0.005

We also estimate the probability to lose a hard interaction event because no primary vertex is reconstructed. We find that the fraction of such events in the MB event sample with jet $p_T > 15$ GeV is about 0.1% and about 0.2% for the $\gamma\gamma + \geq 1$ jet events in data. Due to the vertex reconstruction algorithm, we may also have an additional reconstructed vertex that passes the vertex requirement. The rate at which this occurs is estimated using $\gamma\gamma + \geq 1$ jet events and $\gamma\gamma + \geq 2$ jets events simulated in MC without the events from random $p\bar{p}$ bunch crossings overlaid (there should not be a second vertex in this case). The probability to have a second vertex is around 0.05%. An analogous estimate for dijet events (with the requirement of ≥ 1 and ≥ 2 jets) returns a probability of around 0.1%.

E. Correction of N_{DI} for the track efficiency requirement

For the DI fraction calculation, we use the CPF algorithm, described in Sec. VIB. The method requires ≥ 2 tracks and returns the highest CPF. The efficiency for the track requirement is calculated similarly to the vertex efficiency for each event-type and then combined with the event type weights. Finally, the estimated number of DI events, N_{DI} , is corrected for the $\epsilon_{N_{trk} \geq 2}$ efficiency which is found to be $\epsilon_{N_{trk} \geq 2} = 0.725 \pm 0.004$.

F. Calculating R_c , σ_{hard} , $N_{1\text{coll}}$ and $N_{2\text{coll}}$

We calculate the numbers of expected events with one $[N_c(1)]$ and two $[N_c(2)]$ $p\bar{p}$ collisions resulting in hard interactions following the procedure of Ref. [22], which uses the hard $p\bar{p}$ interaction cross section $\sigma_{\text{hard}} = 44.76 \pm 2.89$ mb. The values of $N_c(1)$ and $N_c(2)$ are obtained from a Poisson distribution parametrized with the average number of hard interactions in each bin of

the instantaneous luminosity, L_{inst} , distribution, $\langle n \rangle = (L_{\text{inst}}/f_{\text{cross}})\sigma_{\text{hard}}$, where f_{cross} is the frequency of beam crossings for the Tevatron [36]. Summing over all L_{inst} bins, weighted with their fractions, we get $R_c = (1/2)(N_c(1)/N_c(2)) = 0.45$. Due to higher instantaneous luminosities, this number is smaller by approximately a factor of 2 compared to that for the data collected earlier as reported in Ref. [22]. Since R_c and σ_{hard} enter Eq. (7) for σ_{eff} as a product, any increase of σ_{hard} leads to an increase of $\langle n \rangle$ and, as a consequence, to a decrease in R_c , and vice versa. Although the measured value of σ_{hard} has a 6% relative uncertainty, due to this partial cancellation of uncertainties, the product $R_c\sigma_{\text{hard}}$ only has a 2.6% uncertainty: $R_c\sigma_{\text{hard}} = 18.92 \pm 0.49$ mb.

VIII. RESULTS

The uncertainty in the JES affects the ratio N_{DI}/N_{DP} in Eq. (7). We assess this uncertainty by raising and lowering JES by 1 GeV to give an uncertainty in σ_{eff} of 13.2%. We use Eq. (7) to obtain σ_{eff} :

$$\sigma_{\text{eff}} = 19.3 \pm 1.4(\text{stat}) \pm 7.8(\text{syst})\text{mb}. \quad (13)$$

The main sources of systematic uncertainties are summarized in Table VIII. The dominant sources are those due to f_{DP} , f_{DI} , and JES.

Figure 6 shows all the measurements of σ_{eff} performed by various experiments up to the present time. One can see that the σ_{eff} obtained by this measurement agrees with the recent D0 measurements [22, 24] and with those obtained by other experiments for processes dominated by $q\bar{q}$ and qg initial states.

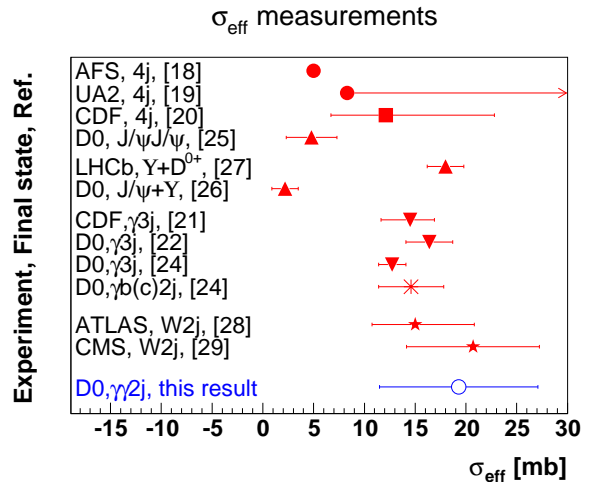


FIG. 6: Existing measurements of the effective cross section, σ_{eff} , compared to the result presented here (AFS: no uncertainty is reported; UA2: only a lower limit is provided). Results of the measurements are grouped by the final state.

TABLE VIII: Systematic and statistical uncertainties (in %). The contributions to the total systematic uncertainty come from uncertainties in the fraction of DP and DI in the one- and two-vertex events samples (f_{DP} and f_{DI}), the ratio of efficiency times acceptance (“EffRatio”), the ratio of photon fractions (“Purity”), JES, and the ratio of the number of events with single and double $p\bar{p}$ hard collisions (“ $R_{\text{c}}\sigma_{\text{hard}}$ ”).

f_{DP}	f_{DI}	EffRatio	Purity	JES	$R_{\text{c}}\sigma_{\text{hard}}$	SystTotal	StatTotal	Total
31.0	18.7	7.1	7.2	13.2	2.6	40.2	6.9	40.8

IX. SUMMARY

We have presented the first measurement of double parton scattering processes in a single $p\bar{p}$ collision with $\gamma\gamma + \text{dijet}$ final states. In the chosen kinematic region, $p_{\text{T}}^{\gamma_1} > 16$ GeV, $p_{\text{T}}^{\gamma_2} > 15$ GeV, $|\eta^{\gamma}| < 1.0$, $|\eta^{\text{jets}}| < 3.5$, and $15 < p_{\text{T}}^{\text{jets}} < 40$ GeV, photon separation $\Delta\mathcal{R} > 0.4$, photon-jet separation $\Delta\mathcal{R} > 0.9$, and jet-jet separation $\Delta\mathcal{R} > 1.4$, we observe that $21.3 \pm 6.7\%$ of events arises from double parton scattering. The parameter σ_{eff} , which characterizes the size of the interaction region in a nucleon, is found to be $\sigma_{\text{eff}} = 19.3 \pm 1.4$ (stat) ± 7.8 (syst) mb.

Acknowledgements

We thank the staffs at Fermilab and collaborating institutions, and acknowledge support from the Department of Energy and National Science Foundation (United States of America); Alternative Energies and Atomic Energy Commission and National Center for Scientific Research/National Institute of Nuclear and Particle Physics

(France); Ministry of Education and Science of the Russian Federation, National Research Center “Kurchatov Institute” of the Russian Federation, and Russian Foundation for Basic Research (Russia); National Council for the Development of Science and Technology and Carlos Chagas Filho Foundation for the Support of Research in the State of Rio de Janeiro (Brazil); Department of Atomic Energy and Department of Science and Technology (India); Administrative Department of Science, Technology and Innovation (Colombia); National Council of Science and Technology (Mexico); National Research Foundation of Korea (Korea); Foundation for Fundamental Research on Matter (The Netherlands); Science and Technology Facilities Council and The Royal Society (United Kingdom); Ministry of Education, Youth and Sports (Czech Republic); Bundesministerium für Bildung und Forschung (Federal Ministry of Education and Research) and Deutsche Forschungsgemeinschaft (German Research Foundation) (Germany); Science Foundation Ireland (Ireland); Swedish Research Council (Sweden); China Academy of Sciences and National Natural Science Foundation of China (China); and Ministry of Education and Science of Ukraine (Ukraine).

-
- [1] P.V. Landshoff and J.C. Polkinghorne, *Calorimeter triggers for hard collisions*, Phys. Rev. D **18**, 3344 (1978).
 - [2] C. Goebel, F. Halzen, and D.M. Scott, *Double Drell-Yan annihilations in hadron collisions: Novel tests of the constituent picture*, Phys. Rev. D **22**, 2789 (1980).
 - [3] F. Takagi, *Multiple Production of Quark Jets off Nuclei*, Phys. Rev. Lett. **43**, 1296 (1979).
 - [4] N. Paver and D. Treleani, *Multiquark scattering and large- p_{T} jet production in hadronic collisions*, Nuovo Cimento A **70**, 215 (1982).
 - [5] B. Humpert, *Are there multiquark interactions?*, Phys. Lett. B **131**, 461 (1983).
 - [6] B. Humpert and R. Odorico, *Multi-parton scattering and QCD radiation as sources of four-jet events*, Phys. Lett. B **154**, 211 (1985).
 - [7] T. Sjöstrand and M. van Zijl, *A multiple-interaction model for the event structure in hadron collisions*, Phys. Rev. D **36**, 2019 (1987).
 - [8] G. Calucci and D. Treleani, *Double parton scatterings in high-energy hadronic collisions*, Nucl. Phys. B, Proc. Suppl. **71**, 392 (1999).
 - [9] G. Calucci and D. Treleani, *Proton structure in transverse space and the effective cross section*, Phys. Rev. D **60**, 054023 (1999).
 - [10] G. Calucci and D. Treleani, *Multiparton correlations and “exclusive” cross sections*, Phys. Rev. D **79**, 074013 (2009).
 - [11] C. Flensburg, G. Gustafson, L. Lonnblad, and A. Ster, *Correlations in double parton distributions at small x* , J. High Energy Phys. 06 (2011) 066.
 - [12] T. Sjöstrand and P. Z. Skands, *Multiple Interactions and the Structure of Beam Remnants*, J. High Energy Phys. 03 (2004) 053.
 - [13] A. M. Snigirev, *QCD status of factorization ansatz for double parton distributions*, Phys. Rev. D **68**, 114012 (2003).
 - [14] V. L. Korotkikh and A. M. Snigirev, *Double parton correlations versus factorized distributions*, Phys. Lett. B **594**, 171 (2004).
 - [15] L. Frankfurt, M. Strikman, and C. Weiss, *Dijet production as a centrality trigger for p-p collisions at CERN LHC*, Phys. Rev. D **69**, 114010 (2004).
 - [16] L. Frankfurt, M. Strikman, and C. Weiss, *Transverse nucleon structure and diagnostics of hard parton-parton processes at LHC*, Phys. Rev. D **83**, 054012 (2011).
 - [17] D. Bandurin, G. Golovanov, and N. Skachkov, *Double*

- parton interactions as a background to associated HW production at the Tevatron, *J. High Energy Phys.*, 04 (2011) 054.
- [18] T. Akesson et al. (AFS Collaboration), *Double parton scattering in pp collisions at $\sqrt{s} = 63$ GeV*, *Z. Phys. C* **34**, 163 (1987).
 - [19] J. Alitti et al. (UA2 Collaboration), *A study of multi-jet events at the CERN $p\bar{p}$ collider and a search for double parton scattering*, *Phys. Lett. B* **268**, 145 (1991).
 - [20] F. Abe et al. (CDF Collaboration), *Study of four-jet events and evidence for double parton interactions in $p\bar{p}$ collisions at $\sqrt{s} = 1.8$ TeV*, *Phys. Rev. D* **47**, 4857 (1993).
 - [21] F. Abe et al. (CDF Collaboration), *Double parton scattering in $p\bar{p}$ collisions at $\sqrt{s} = 1.8$ TeV*, *Phys. Rev. D* **56**, 3811 (1997).
 - [22] V. M. Abazov et al. (D0 Collaboration), *Double parton interactions in $\gamma + 3$ jet events in $p\bar{p}$ collisions at $\sqrt{s} = 1.96$ TeV*, *Phys. Rev. D* **81**, 052012 (2010).
 - [23] V. M. Abazov et al. (D0 Collaboration), *Azimuthal decorrelations and multiple parton interactions in $\gamma + 2$ jet and $\gamma + 3$ jet events in $p\bar{p}$ collisions at $\sqrt{s} = 1.96$ TeV*, *Phys. Rev. D* **83**, 052008 (2011).
 - [24] V. M. Abazov et al. (D0 Collaboration), *Double parton interactions in $\gamma + 3$ jet and $\gamma + b/c$ -jet + 2 jet events in $p\bar{p}$ collisions at $\sqrt{s} = 1.96$ TeV*, *Phys. Rev. D* **89**, 072006 (2014).
 - [25] V. M. Abazov et al. (D0 Collaboration), *Observation and studies of double J/ψ production at the Tevatron*, *Phys. Rev. D* **90**, 111101 (R) (2014).
 - [26] V. M. Abazov et al. (D0 Collaboration), *Evidence for simultaneous production of J/ψ and Υ mesons*, *Phys. Rev. Lett.* **116** (2016) 8, 082002.
 - [27] R. Aaij et al. (LHCb Collaboration), *Production of associated Υ and open charm hadrons in pp collisions at $\sqrt{s} = 7$ and 8 TeV via double parton scattering*, arXiv:1510:05949.
 - [28] G. Aad et al. (ATLAS Collaboration), *Measurement of hard double-parton interactions in $W(\rightarrow l\nu) + 2$ -jet events at $\sqrt{s} = 7$ TeV with the ATLAS detector*, *New J. Phys.* **15**, 033038 (2013).
 - [29] S. Chatrchyan et al. (CMS Collaboration), *Study of double parton scattering using $W + 2$ -jet events in proton-proton collisions at $\sqrt{s} = 7$ TeV*, *J. High Energy Phys.*, **03** (2014) 032.
 - [30] R. Aaij et al. (LHCb Collaboration), *Observation of double charm production involving open charm in pp collisions at $\sqrt{s} = 7$ TeV*, *J. High Energy Phys.* **06** (2012) 141.
 - [31] The polar angle θ and the azimuthal angle ϕ are defined with respect to the positive z axis, which is along the proton beam direction. Pseudorapidity is defined as $\eta = -\ln[\tan(\theta/2)]$. η_{det} and ϕ_{det} are the pseudorapidity and the azimuthal angle measured with respect to the center of the detector.
 - [32] M. Drees and T. Han, *Signals for Double Parton Scattering at the Fermilab Tevatron*, *Phys. Rev. Lett.* **77**, 4142 (1996).
 - [33] V. M. Abazov et al. (D0 Collaboration), *Hard Single Diffraction in $p\bar{p}$ Collisions at $\sqrt{s} = 630$ and 1800 GeV*, *Phys. Lett. B* **531**, 52 (2002).
 - [34] V. M. Abazov et al. (D0 Collaboration), *Observation of diffractively produced W and Z bosons in $p\bar{p}$ collisions at $\sqrt{s} = 1800$ GeV*, *Phys. Lett. B* **574**, 169 (2003).
 - [35] V. M. Abazov et al. (D0 Collaboration), *Probing Hard Color-Singlet Exchange in $p\bar{p}$ Collisions at $\sqrt{s} = 630$ GeV and 1800 GeV*, *Phys. Lett. B* **440**, 189 (1998).
 - [36] V. M. Abazov et al. (D0 Collaboration), *The upgraded D0 detector*, *Nucl. Instrum. Methods Phys. Res. A* **565**, 463 (2006).
 - [37] M. Abolins et al., *Design and implementation of the new D0 level-1 calorimeter trigger*, *Nucl. Instrum. Methods Phys. Res. A* **584**, 75 (2008).
 - [38] R. Angstadt et al., *The layer 0 inner silicon detector of the D0 experiment*, *Nucl. Instrum. Methods Phys. Res. A* **622**, 298 (2010).
 - [39] T. Andeen et al., *The D0 Experiment's Integrated Luminosity for Tevatron Run IIa*, FERMILAB-TM-2365, 2007.
 - [40] V. M. Abazov et al. (D0 Collaboration), *Measurement of the differential cross section of photon plus jet production in $p\bar{p}$ collisions at $\sqrt{s} = 1.96$ TeV*, *Phys. Rev. D* **88**, 072008 (2013).
 - [41] V. M. Abazov et al. (D0 Collaboration), *Electron and Photon Identification in the D0 Experiment*, *Nucl. Instrum. Methods Phys. Res. Sect. A* **750**, 78 (2014).
 - [42] V. M. Abazov et al. (D0 Collaboration), *Measurement of the differential cross sections for isolated direct photon pair production in $p\bar{p}$ collisions at $\sqrt{s} = 1.96$ TeV*, *Phys. Lett. B* **725**, 6 (2013).
 - [43] G. C. Blazey et al., arXiv:0005012.
 - [44] V. M. Abazov et al. (D0 Collaboration), *Jet energy scale determination in the D0 experiment*, *Nucl. Instrum. Methods A* **763**, 442 (2014).
 - [45] T. Gleisberg et al., *Event generation with Sherpa 1.1*, *J. High Energy Phys.* 02 (2009) 007.
 - [46] T. Sjöstrand, et al., *PYTHIA 6.4 Physics and Manual*, *J. High Energy Phys.* 05 (2006) 026.
 - [47] R. Brun and F. Carminati, *CERN Program Library Long Writeup W5013*, 1993, unpublished.
 - [48] R. Barlow and C. Beeston, *Fitting using finite Monte Carlo samples*, *Comp. Phys. Comm.* **77**, 219 (1993).
 - [49] R. Hamberg, W. L. van Neerven, T. Matsuura, *A complete calculation of the order α_s^2 correction to the Drell-Yan K -factor*, *Nucl. Phys.* **B359**, 343 (1991) [Erratum-ibid. **B644**, 403 (2002)].